Coalescence of Water Drops at an Oil−Water Interface Loaded with Microparticles and Surfactants

Esteban Calvo,*,[†],[‡][iD] Erik de Malmazet,[§],[#] Frédéric Risso,[§],[∥][iD] and Olivier Masbernat[∥],[⊥]

[†]Área de Mecánica de Fluidos, Escuela de Ingeniería y Arquitectura, Universidad de Zaragoza, María de Luna, 3, 50018, Zaragoza, Spain

[‡]Laboratorio de Investigación en Fluidodinámica y Tecnologías de la Combustión—LIFTEC, CSIC, Universidad de Zaragoza, María de Luna, 10, 50018, Zaragoza, Spain

[§]Institut de Mécanique des Fluides de Toulouse (IMFT), Université de Toulouse, CNRS, 2 Allée du Professeur Camille Soula, 31400 Toulouse, France

[∥]FR FERMaT, Université de Toulouse, CNRS, INPT, INSA, UPS, c/o Laboratoire de Génie Chimique, 118 route de Narbonne, 31062 Toulouse, France

[⊥]Laboratoire de Génie Chimique (LGC), Université de Toulouse, CNRS, 4 Allée Emile Monso CS 84234, 31432 Toulouse cedex 4, France

Ⓢ *Supporting Information*

ABSTRACT: This work investigates the coalescence of water droplets settled on a water−oil interface in the presence of microparticles and surfactant. The successive stages of the coalescence process, including interstitial film formation, drainage, rupture, and retraction, are analyzed in detail. This leads us to distinguish between contrasted situations depending on the nature of the surfactant and its affinity with the microparticles. Hydrophilic particles have been previously shown to promote coalescence by means of a bridging mechanism. In that case, coalescence is a deterministic process that lasts the time required for the drainage to make the film thickness equal to the size of the particles. However, the present study shows how surfactants can totally change the effect of the particles upon coalescence. When surfactant both stabilizes the water−oil interface and adsorbs onto the particles, the bridging mechanism is inhibited and the coalescence becomes a random process. Since molecular forces between facing film interfaces are not attractive, thermal fluctuations are required to initiate the formation of a hole in the adsorbed surfactant layer. Provided the surfactant concentration in the bulk is large enough to ensure that the interfaces are close to saturation, the coalescence is delayed by a stochastic time interval and the drop coalescence becomes a Poisson process. These results shed a new light on the mechanisms of droplet coalescence in complex industrial applications where surfactant and particles are present, either purposely added or present as uncontrolled contaminants.
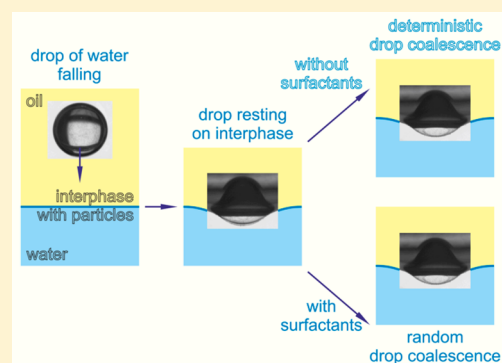
1. INTRODUCTION

Coalescence is a key phenomenon in a wide range of industrial applications, such as phase separation in gravity or centrifuge settlers, sprays, foams, or emulsions. While this phenomenon has been extensively studied over the last century in many phase systems,[1−28] it still remains unpredictable and difficult to scale for a given application. In chemical engineering a classical approach of the coalescence process is to model the kinetics of drainage of the drop−interface or drop−drop interstitial film, accounting or not for the disjoining pressure or Marangoni stress.[5,15,18] These models predict a deterministic evolution of the film drainage, which can be verified experimentally, with mobile or immobile interfaces. Combining these models with the notion of critical thickness, below which attractive van der Waals force triggers the film rupture, they also predict a given coalescence time (or film lifetime or rest time) for a given set

of phase properties and flow parameters, which is not often observed in experiments, excepted in the rare case of clean interfaces. This is particularly true for liquid−liquid systems, and there are two main reasons for this. First is that, for most of the systems studied, coalescence is a stochastic process, which is controlled in its final stage by the thermal motion of adsorbed surface-active species at the interface.[2−8] The second reason is that, in industrial processes, the composition of the interface is rarely known and is often out of thermodynamic equilibrium. More generally this indeterminate composition of the interface is a central question in the determination of

interfacial momentum transfer for the prediction of slip velocity or drop deformation in liquid−liquid dispersions.

In a recent study, de Malmazet et al.[29] studied experimentally the effect of the presence of microparticles (μ-particles) on contaminated oil−water interfaces upon the interstitial film rupture, leading to drop−interface coalescence. The main finding of this study is that these μ-particles can trigger the coalescence process at early stages of the film drainage, shifting the randomness of the film lifetime toward a much more deterministic variable, which is found to be a growing function of drop diameter as when driven by the film drainage kinetics of deformable clean drops.[16]

One interesting feature of that experiment was the in situ measurement of the interfacial tension of the oil−water interface at the location where the drop was resting prior to coalescence. The knowledge of this quantity at the location of the coalescence event turned out to be relevant to support the idea that the onset of coalescence was driven by a bridging mechanism induced by the μ-particles trapped on the interface. As the interface was aging, its surface tension was found to decrease due to a growing contamination from surface-active species adsorbing from the oil phase or released from the particles. In the presence of particles, the coalescence time was found to decrease with the surface tension, a trend that is opposite in the film drainage theory, for partially mobile or immobile interfaces. In turn, this trend was consistent with a particle-induced bridging mechanism due to the increase of the contact angle of water on particles as the interfacial tension was decreasing. Indeed, the increase of contact angle (but remaining smaller than $\pi/2$) was increasing the height of immersion of the particle in the oil phase, and was therefore possibly responsible for an earlier occurrence of the bridging effect, leading to an overall decrease of the coalescence time.

For a given state of contamination of the interface (i.e., at a given age of the interface), the dynamics of a bridging-induced coalescence can be roughly depicted as a film drainage process until a critical thickness equal to the height of immersion of the particle in the film phase. However, even if μ-particles make the coalescence process become much more deterministic, film lifetime data scattering is still present, due to the polydispersity of microparticles and to the stochastic nature of contact angle for any three-phase system. The importance of the wetting properties (contact angle) of the μ-particles at the interface on the bridging mechanism naturally raises the question of the sensitivity of this mechanism to the presence of an adsorbed layer of surfactants, which is addressed in the present paper.

The present work extends the study de Malmazet et al.[29] with the same phase system (mineral oil and water), investigating the combined effect of surfactants with that of the microparticles on the different stages of the coalescence process. In the former study of de Malmazet et al.,[29] the interface was contaminated with surface-active impurities contained in the oil phase (and maybe also from some biological contamination of the water phase at long aging time), adsorbing at the oil−water interfaces or at the particle surface. In the present study, a significant concentration of nonionic surfactant was added in water in order to control the loading of the oil−water interfaces, at least for young interfaces. Two bulk concentrations of a nonionic surfactant were investigated (Tween 80), respectively corresponding to a nonsaturated and a nearly saturated interface. In both cases, glass μ-particles were introduced on the settling drop interface and on the oil−water plane interface. Note that the interfacial

system studied is complex, loaded with μ-particles, surfactants, and other contaminants, mimicking the conditions of most of real applications, such as oil recovery processes.

As in the work of de Malmazet et al.,[29] different stages of the coalescence process have been studied: the water drop settling in the oil phase toward the water−oil interface, the drainage time of the interstitial film, the coalescence time (or lifetime) of the film, i.e., the time elapsed between the end of the film drainage and the occurrence of the film rupture, and finally the dynamics of the film retraction at the onset of coalescence.

The paper is divided into five sections. In section 2, the experimental setup, materials, as well as the measurement techniques and procedures are presented. Section 3 details the experimental results and the features of the observed coalescence events. The physical interpretation of the experimental results is proposed in section 4. The comparison with the results of de Malmazet et al.[29] is of crucial importance to unveil the mechanisms involved in the coalescence process. In section 5, the main results and findings of this study are summarized.

2. DESCRIPTION OF THE EXPERIMENT

In this section, an overview of the drop−interface coalescence device, phase properties, and measurement techniques is given. The experimental setup is the same as that used in de Malmazet et al.,[29] and the materials (liquids and micro-particles) come from the same batches.

2.1. Experimental Setup and Phase Properties. In this experiment, drops of water are released in a volume of oil resting upon a volume of water, and forming a steady interface. The drop−interface interaction is observed inside a transparent square chamber of inner dimensions 20 × 20 × 45 mm^3 (Figure 1). The lateral walls of the chamber are made of
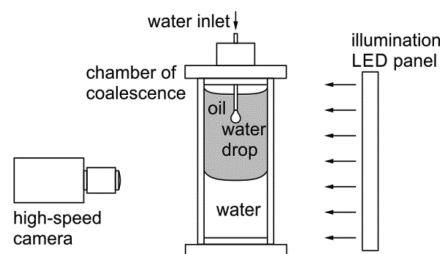

Figure 1. Schematic of the experimental setup.

optical grade glass, and both the top and bottom sides are made of stainless steel. Water drops are injected by means of a capillary tube located at the top of the coalescence chamber and connected to a microliter syringe manually operated. A water drop of a prescribed volume is generated at the capillary tip and detaches from the capillary when applying a mild jolt, allowing the injection of drops ranging from 1 to 4 or 5 mm in diameter. The whole experiment is inside a room maintained at constant temperature of 20 °C.

Prior to each experimental campaign, the coalescence chamber is disassembled and all parts are carefully washed with distilled water, acetone, heptane, and toluene, in order to remove residues adhering to the inner walls. The bottom of the coalescence chamber is then filled with distilled water and the top is filled with a lighter mineral oil from the top (Figure 1). The N100 oil used in this study is a viscosity standard manufactured by Paragon Scientific. This mineral oil is a

mixture of hydrocarbon chains ranging from C15 to C40, of unknown composition. The density and viscosity reported by the manufacturer are ρ_O = 865.7 kg/m³ and μ_O = 283.6 mPa·s, respectively (at 20 °C). This oil contains amphiphilic compounds as revealed by the value of its surface tension with water (below 40 mN/m, Figure 2b). Water properties at 20 °C are ρ_W = 998.2 kg/m³ and μ_W = 1.002 mPa·s.
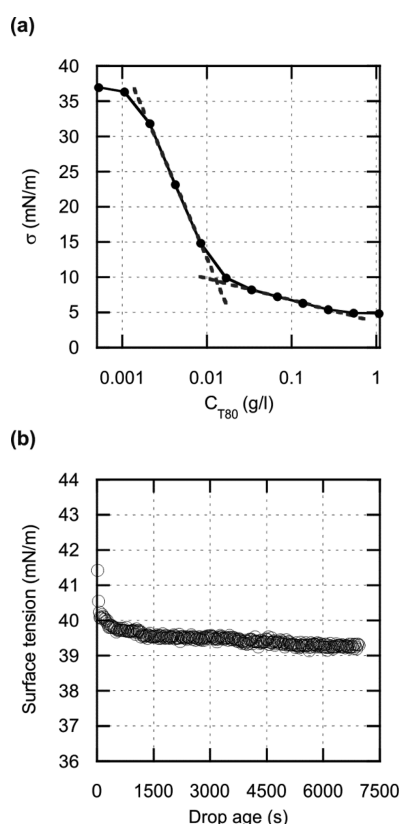

Figure 2. (a) Dependence of interfacial tension on Tween 80 concentration. (b) N100 oil–pure water interfacial tension as a function of time.

The surfactant used in this study is polysorbate 80 (or Tween 80 from Sigma-Aldrich), which is a nonionic surfactant preferentially soluble in water. Its molecular weight is 1310 g/mol. Tween 80 (T80) is added in the same concentration to both the water in the coalescence chamber and the injected drops. Figure 2a shows on a semilog scale the interfacial tension between water and N100 oil at equilibrium as a function of T80 bulk concentration (measured with a Krüss DSA100 pendant-drop tensiometer). The decay of the surface tension with increasing concentration of T80 exhibits two regimes with an abrupt change of slope at a concentration of 0.013 g/L (~10 μM) and then stabilizes around 0.3 g/L (~230 μM). Because of this change of slope, it is not possible to fit this curve with a single Gibbs isotherm, and provide a reasonable estimation of the surface excess of T80 at saturation. This peculiar behavior of the surface tension with concentration in T80 may result from a heterogeneous chemical composition of T80 (length of each ethylene oxide group attached to the sorbitan head) or from a possible degradation of T80 due to a slow autoxidation mechanism.[30] It may also result from the competitive adsorption of other surface-active species contained in the oil phase[31] or from a

restructuration of adsorbed T80 at the interface.[32] The used tensiometer can measure the surface tension of a drop interphase with time. It decreases even for a drop of pure water (Figure 2b), suggesting the presence of other surface-active contaminants in the N100 oil. However, the evolution of equilibrium surface tension displayed in Figure 2a allows us to select, for the purpose of the present study, two significant but contrasted concentrations in surfactant, one well below the interface saturation (C_{T80} = 0.011 g/L) and a second, 10 times larger, closer to the saturation (C_{T80} = 0.11 g/L). Respective values of interfacial tension between N100 and surfactant solutions at equilibrium are 13.1 and 6.65 mN/m.

The same hollow glass spherical μ-particles as those used in de Malmazet's experiments are added to the injected water drops. Their size distribution is rather narrow and centered around 10 μm (Figure 3). Since they are small, light, and
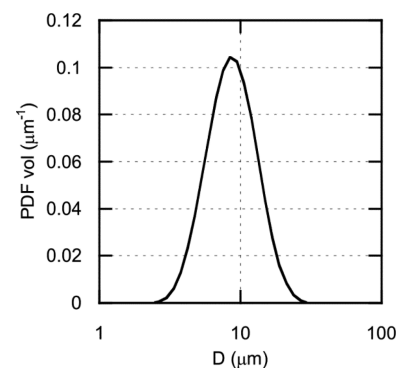

Figure 3. Size distribution of the hollow glass microspheres.

preferentially wetted by water, these μ-particles are easily trapped at the oil–water interface. As in de Malmazet et al.'s experiments, the injected drops are loaded with these particles transporting them to the plane oil–water interphase after successive coalescence events. In de Malmazet et al.'s experiments (without T80), this particle input was performed during the first three days of the experimental campaign. For the following experiments, as these particles remained attached and stable on the interface, it was not necessary to keep on supplying particles by means of the injected drops. However, in the presence of surfactants, it was observed that the glass particles already present at the interface were pushed away from the zone of contact after a drop free of particles had coalesced, leaving the impact zone free of particles. Therefore, in order to maintain a suitable amount of particles on the interface, only drops containing particles were injected in the cell throughout all the campaign.

The settling and coalescence process of water drops have been observed and recorded using a high-speed camera (PCO Dimax). Its low noise CMOS sensor has a resolution of 2016 × 2016 pixels and the frame rate is 1279 fps with a full-size image. A variable high-luminosity LED panel is placed behind the cell for backlighting.

Two experimental campaigns were carried out with the two aforementioned surfactant concentrations (C_{T80} = 0.011 g/L and C_{T80} = 0.11 g/L). Both the water bulk and the injected drops came from the same T80–water solution, guaranteeing the same concentration. For each campaign, the injected drop size ranged between 2.5 and 4.5 mm, corresponding to particle Reynolds numbers at terminal velocity (Figure 5) of 7.6 × 10^{-3} and 4.1 × 10^{-2}, respectively. The duration of both

campaigns was about 2 weeks. A total number of 272 drops were released during the first campaign, and 87 drops were released during the second.

2.2. Measured Quantities. Image processing allows the measurement of a wide set of quantities. After the calibration of images using the width of the coalescence cell, drop size d and settling velocity v_T can be accurately determined. The coalescence time t_C is defined as the time interval between the instant of drop contact with the water−oil interface and the onset of coalescence (pinhole formation at the interface). Both t_C and the time of the drop impact with the water−oil interface, t_I, are determined using the internal clock of the camera and an external chronometer. The origin of time ($t =$ 0) corresponds to the filling of the coalescence cell with both liquids (water and oil). Using this origin, the temporal coordinate corresponds to the age of the water−oil interfaces in the cell, which is the relevant time scale for the adsorption process of surfactants.

Finally, the part of the drop volume immersed in the water bulk at the interface (the spherical cap in Figure 7b) and the geometry of the interface around the drop allow the measurement of the interfacial tension of the water−oil plane interface with time, following a procedure similar to that developed by de Malmazet et al.[29] This method is accurate enough to determine the true interfacial tension during the coalescence process. Note that, as the cell windows are made of (hydrophilic) glass, a rising meniscus develops at these walls (Figure 1), causing a severe optical distortion of the upper side of the images, as illustrated in Figures 4b,c,d and 7. However, below the meniscus images are not distorted and interface shape can be properly analyzed.
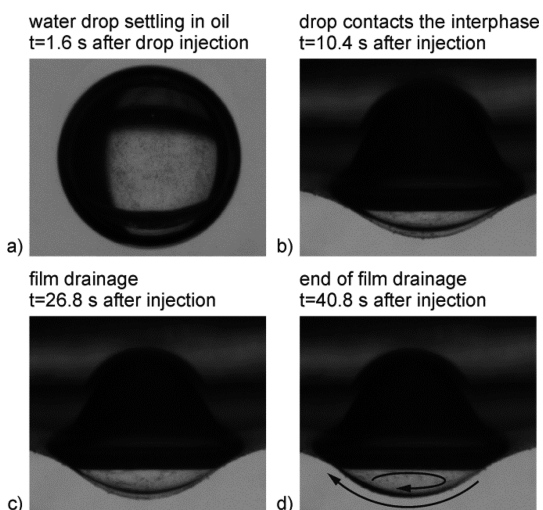

Figure 4. Drop settling and film drainage for drop 137, campaign 1. Time origin is at drop injection. In (d) arrows indicate the direction of the drainage and the motion pattern at the film−drop interface.

3. EXPERIMENTAL RESULTS

The different stages of the coalescence process have been investigated, from the drop injection to the final coalescence with the water bulk.

3.1. Drop Settling, Formation of Drop−Interface Film, and Film Drainage. The first stages of the coalescence process are illustrated in Figure 4: the drop settling (Figure 4a), interface deformation and film formation (Figure 4b), and

the drainage of the film (Figure 4c,d). Drop diameter $d = 2r$, its terminal settling velocity v_T, and the film drainage time are determined from these videos. In the range of particle Reynolds number investigated, the Capillary number ($Ca = \mu_O v_T / \sigma_{OW}$) ranges between 0.022 and 0.13, so the drop shape remains quasi-spherical (Figure 4a).

The drop terminal velocity in the cell as a function of drop diameter is reported in Figure 5. It is the same curve as
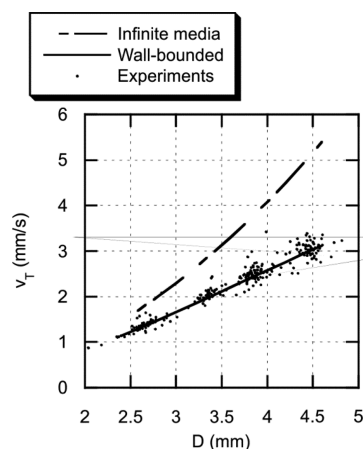

Figure 5. Drop terminal velocity: experimental data (black dots), theoretical values in an infinite (dashed line), or a wall-bounded (continuous line) medium.

previously determined by de Malmazet et al. for all cases studied (i.e., including both T80 concentrations). The evolution is well-fitted by the correlation of Miyamura et al.[33] for solid spherical particles settling in a wall-bounded medium (which accounts for the ratio between drop diameter and cell width). This was expected since it is well-known that a small amount of surfactants can immobilize the interface and kill internal recirculation within the drop.

When the drop approaches the water−oil plane interface, both the drop shape and the interface deform under the action of the drop apparent weight, and then the drop rests on the deformed interface, giving rise to the development of an interstitial film (Figure 4b). Videos showed that this film was drained in two steps. Initially, the film remains quasi-static with a slow drainage rate. Parts b and c of Figure 4 show the film at t = 10.4 and 26.8 s, respectively, after the drop injection. It is nearly unchanged during this period; the maximum thickness is at the center (∼0.1 mm) whereas it is much thinner at the periphery.

About 20 or 30 s later, the film begins to drain quickly. Figure 4c,d shows an appreciable thinning of the film during a time lapse similar to the first step. The motion of the particles attached to the film interphases allows us to visualize a nonaxisymmetric flow pattern. That is, oil does not drain symmetrically through the whole film periphery but through a given azimuthal position, generating two vortices on both sides of the film interfaces. This asymmetric drainage is illustrated in Figure 4d, where the film is draining through the left side of the film rim. This scenario has not been observed previously by de Malmazet et al.,[29] and is likely to be driven by strong Marangoni effects that develop on the interfaces. At the end of this second draining stage, the oil film remains very thin and stable, suggesting that the surfactant concentration on the film surface is almost uniformly distributed.

The drainage time is defined as the time elapsed between the film formation and the end of the film drainage, characterized by the cancellation of any convective flow at the interface. This drainage time has been reported in Figure 6 for both
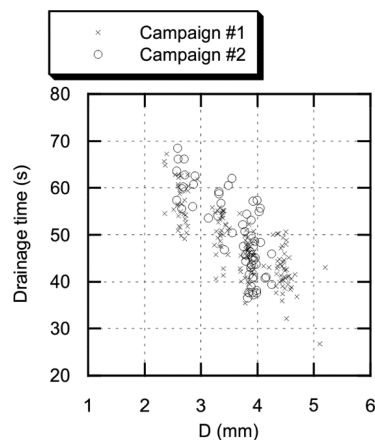

Figure 6. Comparison of the first drainage time: first and second campaigns.

campaigns as a function of drop diameter. Due to the contribution of Marangoni flow instability leading to an asymmetric drainage, and to the estimation of the end of the film drainage, a noticeable scattering of the data is observed on this curve. Despite this, an overall trend is clearly emerging for both experimental campaigns: the film drainage time decreases with the drop size, a trend opposite to what is predicted with classical film drainage models.

3.2. Latency Period and Film Rupture. Once the drainage is complete, a large latency phase is observed prior to the occurrence of film breakup (Figure 7c). During this
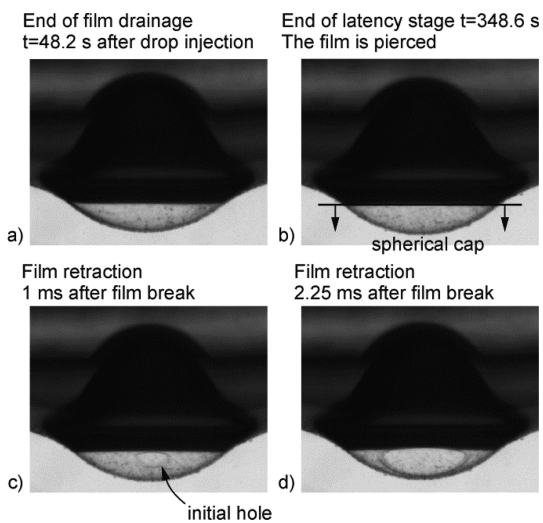

Figure 7. Latency period (a and b), onset of film rupture (c), and film retraction (d) for drop 137, campaign 1.

time, the remaining thin film is stable without any detectable thinning or interfacial motion as shown by the comparison of images of Figure 7a taken at 50 s and Figure 7b, taken 300 s later. For the drop shown in Figure 7, the latency stage lasted about 5 min. The measurement of the surface tension of the water−oil interface at the contact zone was performed during

this latency period. For a quiet drop and a thin interstitial film, the drop volume submerged in the oil bulk must be a spherical cap[34,35] as shown in Figure 7b.

The film rupture begins with the formation of a small pinhole that quickly enlarges (Figure 7c,d). We measured the elapsed time between the drop impact on the interface and the film rupture, and this time was defined as the coalescence time (t_C). Since the film drainage time is much shorter than the coalescence time, t_C measures in essence the duration of the latency period.

In the images of Figure 8, the particles attached to the film interface are visualized during both campaigns. It can be
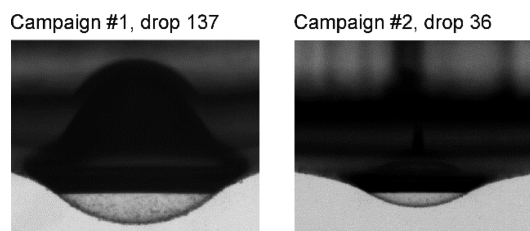

Figure 8. Illustration of interface loading in particles during campaigns 1 and 2.

observed that the concentration of particles on the film interface is larger in the first campaign than in the second, as well as the ability of these particles to aggregate at the interface.

The duration of this latency phase is random and independent of the drop diameter for both surfactant concentrations. Figure 9 shows that it spans over more than 2 orders of magnitude, ranging from a few to several thousand seconds.
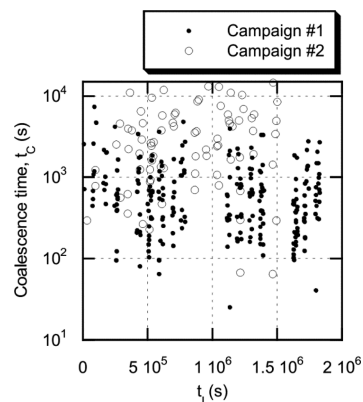
Figure 9. Evolution of coalescence time with interface aging for both experimental campaigns. The origin of time corresponds to the filling of the coalescence cell.

Figure 10 shows the mean coalescence time and its standard deviation as a function of drop volume. No clear relation between these two quantities is observed. The mean coalescence time is 3−4 times larger at the higher T80 concentration (campaign 2) than at the lower one (campaign 1). In both cases, the mean and the standard deviation of the coalescence time (t_C) are quite similar, suggesting an exponential probability distribution for t_C. The cumulative distribution function (CDF) of t_C can be fitted by the following function:

Figure 10. Mean and standard deviation of coalescence time as a function of drop volume for both surfactant concentrations.

$$\text{CDF}(t_C) = \begin{cases} 1 - \exp\left(-\dfrac{t_C - t_0}{\tau_C}\right) & \text{if } t_C \geq t_0 \\ 0 & \text{if } t_C < t_0 \end{cases} \quad (1)$$
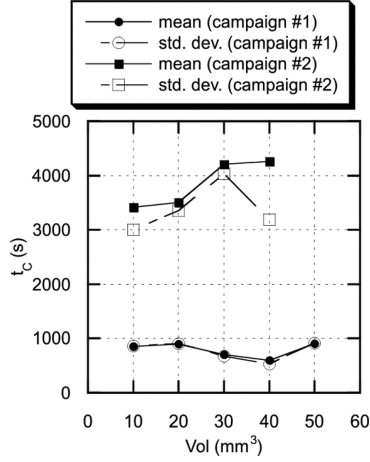
Here, t_0 is the shifted origin of the coalescence time. The exponential constant time (τ_C) is equal to the mean value of t_C minus the time shift t_0. The shift t_0 accounts for the film drainage stage (of the order of a few tens of seconds). Figure 11 compares the experimental and fitted CDFs for the two tested surfactant concentrations. Estimated values of t_0 and τ_C are reported in Table 1. The mean coalescence time strongly depends on the surfactant concentration, displaying a factor of 5 between the larger and the lower surfactant concentrations.

The memoryless property characterizes a Poisson process with an exponential cumulative distribution. The probability that the film breaks during a time interval $(s, s + L)$ does not depend on s but only on its length L, given that the drop had not coalesced before s. This implies that the film seems to experience no "aging" during the latency phase.

However, it can be observed in Figure 10 that the exponential fit of eq 1 is not as good in campaign 1 (Figure 11a) as in campaign 2 (Figure 11b). The fit can be greatly enhanced (Figure 12) considering a piecewise exponential function over three time intervals:

$$\text{CFD}(t_C)$$
$$= \begin{cases} 0 & \text{if } t_C < t_0 \\ 1 - \exp\left(-\dfrac{t - t_0}{\tau_1}\right) & \text{if } t \in (t_0, t_1) \\ 1 - \exp\left(-\dfrac{t_1 - t_0}{\tau_1}\right)\exp\left(-\dfrac{t - t_1}{\tau_2}\right) & \text{if } t \in (t_1, t_2) \\ 1 - \exp\left(-\dfrac{t_1 - t_0}{\tau_1}\right)\exp\left(-\dfrac{t_2 - t_1}{\tau_2}\right)\exp\left(-\dfrac{t - t_2}{\tau_3}\right) \\ \qquad \text{if } t > t_2 \end{cases} \quad (2)$$

The time constant τ_i is reported in Table 2 for the three interval times selected. The inverse of τ_i is the mean coalescence rate in each time interval. Values of Table 2 reveal that the coalescence rate decreases with time. Therefore, the drop is less prone to break as its residence time on the

(a) Campaign #1
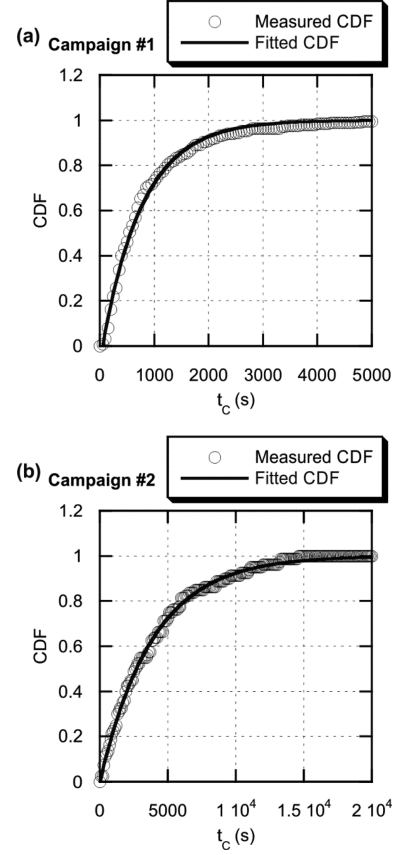
(b) Campaign #2

Figure 11. Cumulative distribution of the coalescence time for (a) campaign 1 ($C_{T80} = 0.011$ g/L) and (b) campaign 2 ($C_{T80} = 0.11$ g/L). Symbols, experimental data (all drop diameters); continuous line, exponential fit.

Table 1. Estimated Parameters of the Coalescence Process in Both Campaigns

campaign	c_{T80} (g/L)	shift t_0 (s)	mean coalescence time τ_C (s)
1	0.011	53.1	741.8
2	0.11	14.5	3873
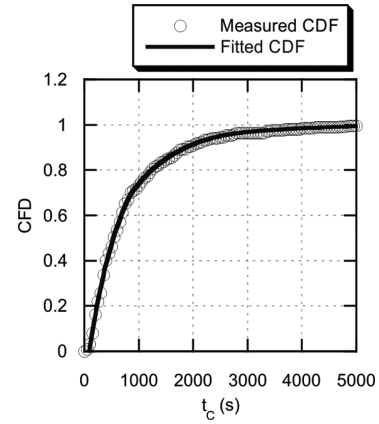
Figure 12. Cumulative distribution function of coalescence time: measured and fitted piecewise exponential distribution. Campaign 1.

interface is increasing, suggesting an evolution of the film interface composition for the lower concentration of surfactant.

Onset of film rupture is caused by the formation of a pinhole in the oil film. The angular position of this initial pinhole, or

Table 2. Time Constant Values of the Coalescence Time Distribution for Campaign 1

| time interval	time constant
(t_0 = 89.9 s, t_1 = 846.2 s)	τ_1 = 642.2 s
(t_1 = 846.2 s, t_2 = 2706 s)	τ_2 = 906.7 s
(t_2 = 2706 s, ∞)	τ_3 = 1354 s

puncture angle ξ, is defined as the difference between the angular location of the puncture and that of the spherical cap submerged in the water bulk (Figure 13). The value of ξ measured on the images is reported as a function of the drop volume in Figure 14b.
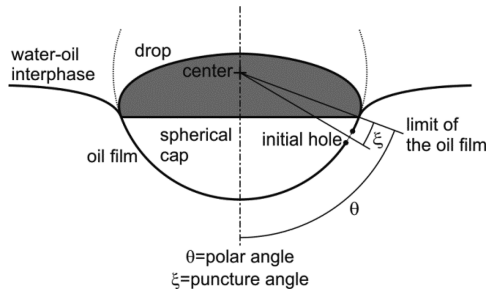

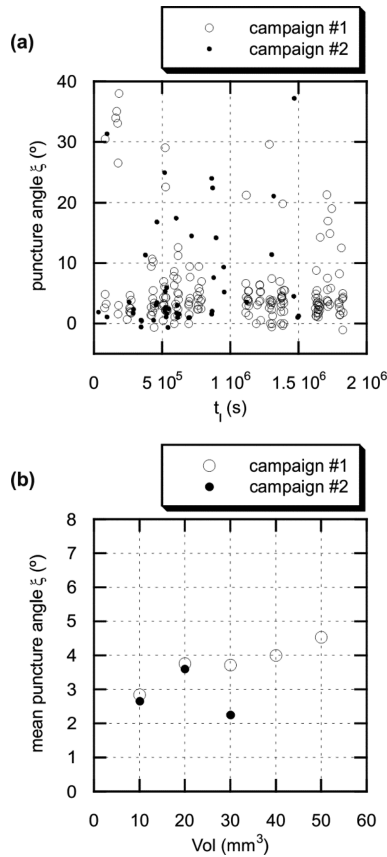**Figure 13.** Definition of puncture angle ξ.

Figure 14. (a) Puncture angle of each injected drop and (b) mean puncture angle for each campaign.

The initial film puncture mainly occurs close to the rim of the film oil (ξ < 10°), but occasionally the film rupture begins at locations closer to the drop axis ($\xi \geq$ 10°). The mean puncture angle is about 3−4° for all size classes in both

campaigns (Figure 14). This suggests that the film thickness is minimum at the outer limit, as previously reported in the literature.[11−14,17,35]

3.3. Film Retraction. The initial hole quickly enlarges (Figure 7c,d), driven by the interfacial tension. The water flows to the bulk through the growing hole and the drop coalesces. Finally, the film disappears and the coalescence ends. The film retraction is very fast, showing a characteristic time scale of about 10 ms.

Videos show that the oil film maintains a quasi-spherical shape during the major part of the retraction stage. Under this assumption, the geometry of the hole could be reconstructed over time. Figure 15 shows the hole expansion for two drops of
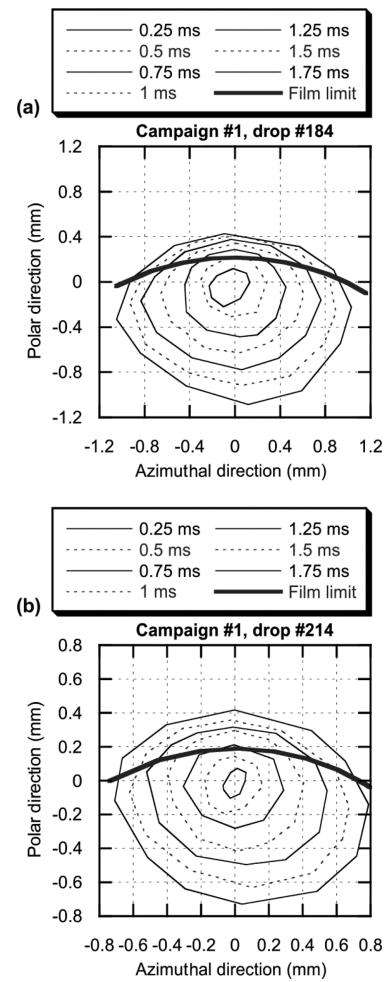
Figure 15. Reconstruction of hole growth versus time during drop coalescence. (a) and (b) correspond to two different drops during campaign 1.

campaign 1 (C_{T80} = 0.011 g/L). The hole is projected on a plane tangent to the spherical film cap at the point of the initial puncture. This point is also the origin of the plots. The thickest gray line corresponds to the film rim, that is, the limit of the bright spherical cap in Figure 7b. Note that when the hole expands beyond the film limit, its shape becomes oval and its reconstruction is not accurate. Qualitatively, the film retraction for campaign 2 is similar.

From the time evolution of the hole geometry, the retraction velocity can be determined. Figure 16 shows a typical example of the temporal evolution of this velocity (measured at the
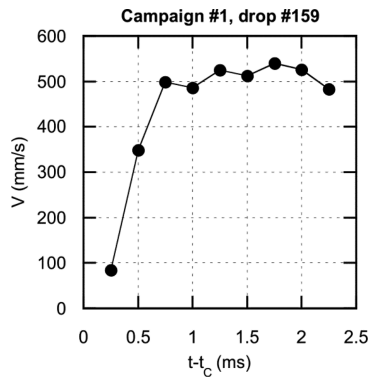
Figure 16. Evolution of film retraction velocity at the lowest point of the hole rim.

lowest point of the hole rim). It starts first to quickly increase and then stabilizes in less than 1 ms, around a constant value.

This limit velocity has been plotted as a function of coalescence time for both campaigns. The difference between both campaigns is significant. In campaign 1, with the lower surfactant concentration, the retraction velocity increases with t_C, whereas these two quantities seem quite uncorrelated with the larger surfactant concentration (campaign 2). The order of magnitude of the limit velocity ranges between 0.5 and 1 m/s.

The maximum retraction velocity is an increasing function of the coalescence time for campaign 1 with the first surfactant concentration (Figure 17a, C_{T80} = 0.011 g/L). However, both variables are not correlated in the second campaign when the surfactant concentration is much higher than the critical micelle concentration (Figure 17b, C_{T80} = 0.11 g/L).
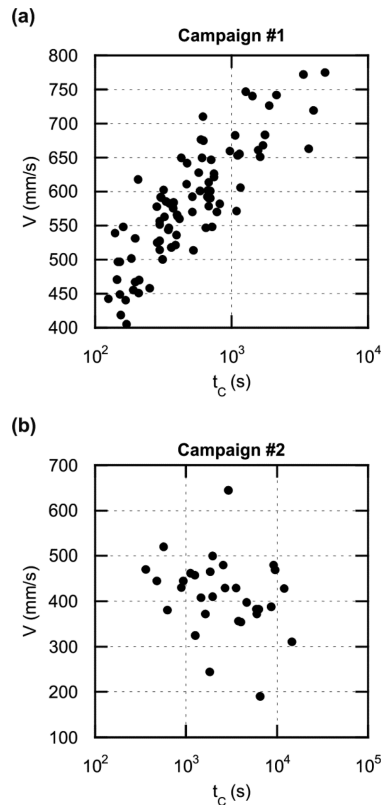

Figure 17. Maximum retraction velocity as a function of drop coalescence time. (a) campaign 1; (b) campaign 2.

3.4. Aging of the Water−Oil Interface. The study of the coalescence process over a long period of time is relevant in many industrial applications. In de Malmazet et al.'s experiments, the oil−water plane interface was aging on a scale of several days due to a growing contamination (issued from N100 oil amphiphilic species and biological contaminants). This aging phenomenon of the interface could be disclosed thanks to the local monitoring of the surface tension of the plane water−oil interface, at the right location where coalescence events took place. In the same way, the long-time evolution of the surface tension of the oil−water interface has been measured in both campaigns.

The measurement of interfacial tension was performed during the latency period, when the drainage stage is over and the film is static. The method is that developed by Malmazet et al.[29] from a force balance along the film shape. The drop volume immersed in the water bulk (Figure 7b) is measured fitting the film shape with a spherical cap. This fitting also provides the slope of the water−oil interface at the outer limit of the oil film. Both magnitudes are needed to derive the interfacial tension.

The evolution of the interfacial tension prior to coalescence is plotted in Figure 18a as a function of interface age and for
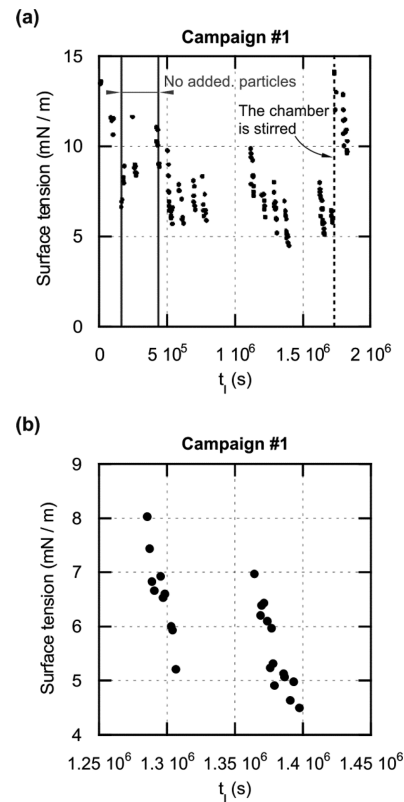
Figure 18. Oil−water interfacial tension versus interface age: (a) whole experiment; (b) zoom between days 16 and 17. Campaign 1, C_{T80} = 0.011 g/L.

the lower surfactant concentration (C_{T80} = 0.011 g/L). The origin of time axis corresponds to the cell filling with oil and water. The first drop and the second drop were injected about 2 h later, and the interfacial tension was found equal to 13.5 mN/m. This value is close to the equilibrium value measured with the tensiometer (Figure 2a, σ = 13.1 mN/m). Then, the continuous injection of drops makes the water−oil interfacial

tension decrease along the day reaching a minimum value around 5 mN/m. This value is approximately the minimum equilibrium value obtained at saturation of the interface (cf. Figure 2a). The interfacial tension then increases when the addition of drops is stopped during the night, due to surfactant desorption from the interface into the liquid bulk. A zoom of Figure 18a reported in Figure 18b clearly illustrates the interface loading during the daytime and its depletion overnight.

This general evolution presents two exceptions. First, there is a sudden increase of the interfacial tension at age 1.73×10^6 s (day 20). It is represented by the vertical dashed line in Figure 18a. The interfacial tension recovers its initial value at the beginning of the campaign ($\sigma \sim 14$ mN/m). At this time, the chamber was gently stirred to remove some microparticles adhering to the cell walls. This stirring renewed the interface, which recovered its initial surface tension.

The second exception occurred between 1.60×10^5 (day 2) and 4.35×10^5 s (day 5), (indicated by the vertical gray lines in Figures 18a and 19). In this period, the interfacial tension was
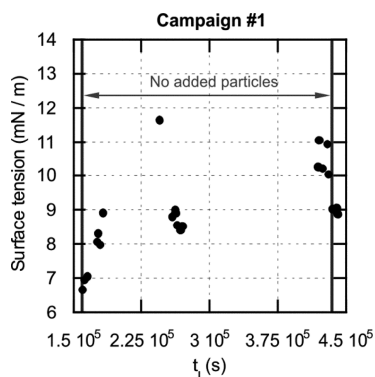

Figure 19. Time evolution of surface tension with particle-free drops. Campaign 1.

increasing instead of decreasing. The drops injected during this period did not contain any particles, following the protocol of de Malmazet et al.[29] It was then observed that, after the drop coalescence, particles moved away from the impact point in contrast with the experiment of de Malmazet et al. Therefore, a zone free of particles appeared at the impact point. In order to avoid this phenomenon, drops containing particles were injected after day 5. Doing so, the depleted zone could be reloaded with μ-particles, and the interfacial tension recovered its aforementioned behavior. In addition, the surface tension dropped immediately after injection of the first drop with microparticles (see the drops after the second vertical gray line in Figure 19). This suggests that the μ-particles supply the interface with additional Tween 80 (and maybe other contaminants) responsible for the daytime decrease of the interfacial tension.

The interface aging was quite different in the second experimental campaign with $C_{T80} = 0.11$ g/L (Figure 20). The interfacial tension did not experience any noticeable daily changes but a small decaying trend of 1 or 2 mN/m over 17 days of aging. In this case, all injected drops did contain μ-particles but the initial concentration of surfactant was close to saturation ($\sigma \sim 6.65$ mN/m), explaining why the interface did not age significantly.
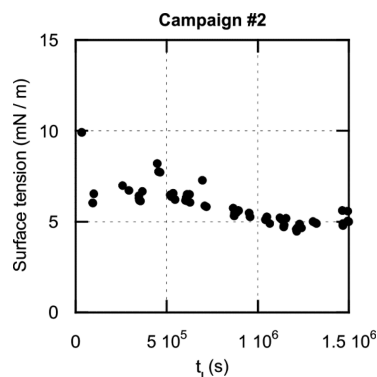

Figure 20. Surface tension versus interface aging during campaign 2. $C_{T80} = 0.11$ g/L.

4. DISCUSSION OF RESULTS

We discuss in this section the physical interpretation of the results and the underlying mechanisms of the drop coalescence. The information provided by the experiments is dense but unfortunately incomplete. Relevant magnitudes remain unknown as the concentration of surface-active compounds at the oil−water interface or at the particle surface, the thickness of the film, or the height of immersion of the μ-particles resting on the interface. A thorough interpretation of the observed phenomena helps to compensate for this lack of information.

The results in de Malmazet et al.[29] showed that the presence of hydrophilic μ-particles at the interface was leading to a deterministic coalescence time, increasing with the drop size. When interfaces are loaded with Tween 80 at significant concentrations, drop coalescence turns out to be a random process even when particles are present and it is no longer correlated with the drop size, as previously observed without surfactants. This difference is explained in section 4.1. Film drainage and film rupture mechanisms are discussed in sections 4.2 and 4.3. Interpretation of the film retraction mechanism (section 4.4) finally provides relevant information about the film interface composition and reinforces the understanding of the coalescence process in the present study, as well as the differences from the observations of de Malmazet et al.[29]

4.1. Interface Structure with Glass Particles and Tween 80. In de Malmazet et al.,[29] the bridging mechanism triggers the drop coalescence. It can be sketched as a film drainage process down to a critical thickness of the order of the particle size. The deterministic feature of the coalescence process and the dependence of the coalescence time with the drop diameter are consistent with this scenario (see eq S7 in the Supporting Information predicts that drainage time increases with drop size). The fact that bridging mechanism is not effective in the present study calls for some interpretation.

The nonionic surfactant Tween 80 adsorbs at oil−water interfaces as well as on high surface energy materials. The adsorption of T80 on glass surfaces has been reported in the literature.[36−39] In the present experiment, a monolayer of that surfactant is probably adsorbed on the particle surface immersed in the oil film as sketched in Figure 21b. In de Malmazet's experiments the interface was loaded with surface-active contaminants that did not or weakly adsorb on glass (Figure 21a), making possible the bridging mechanism of film interfaces, whereas the presence of a monolayer of Tween 80
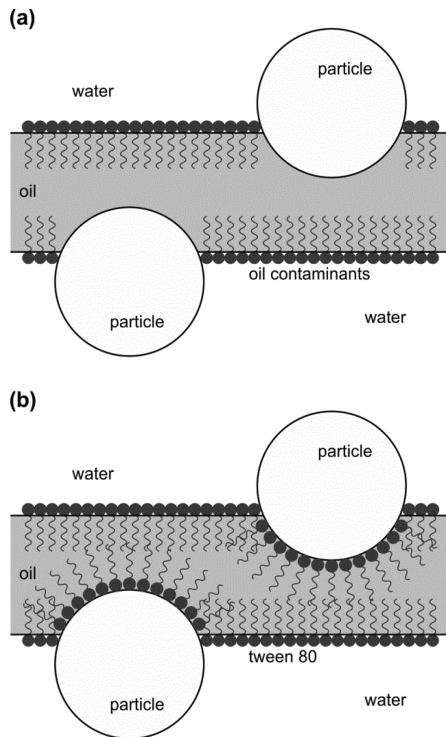
Figure 21. Sketch of structure of adsorbed monolayers at film interfaces with particles: (a) surface-active species nonadsorbing on glass surface; (b) Tween 80 predominately adsorbed.

on the particle surface screens out this bridging effect. If the structure of the adsorbed layer on the particle surface is comparable to that present on the film interface, the film interfaces will be uniformly covered by surfactants. Hence, when the film is thinning, film interfaces will then feel the same energy barrier, with or without particles, explaining the deactivation of the bridging mechanism. Probably, steric effects of the hydrophobic tails stabilize the film.

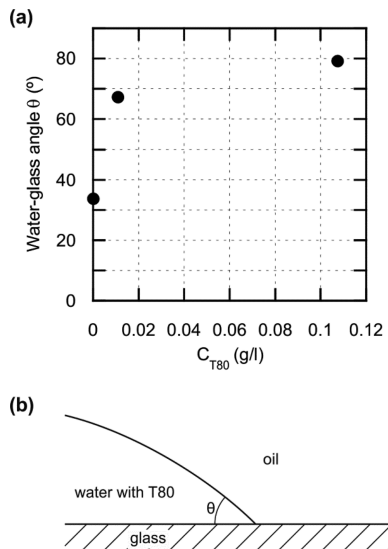There is additional experimental evidence about the adsorption of Tween 80 on the glass surface. Figure 22

Figure 22. Water−glass contact angle as a function of surfactant concentration.

shows the contact angle θ of a water drop on a glass substrate immersed in N100 oil for the T80 concentrations tested in both campaigns. It was measured using the Krüss tensiometer. The contact angle increases as the concentration of Tween 80 increases, tending toward 90°.

The Young−Dupré equation gives the equilibrium contact angle.

$$\cos \theta_{WGO} = \frac{\sigma_{GO} - \sigma_{GW}}{\sigma_{WO}} \tag{3}$$

In this expression, σ is the interfacial tension with the subscripts denoting the corresponding surfaces: "W" for water, "G" for glass, and "O" for oil. As σ_{WO} decreases from 37 mN/m for pure water to 5 mN/m close to the saturation, the numerator $\sigma_{GO} - \sigma_{GW}$ must decrease with a higher rate than σ_{WO}. This suggests a substantial adsorption of T80 at the particle surface, especially at the GO interface. Tween 80 makes the glass particles less hydrophilic, but still preferentially wetted by water, and T80 adsorb on their surface. This increase of water−glass contact angle with T80 surface excess can explain why there are fewer particles present on the drop interface when the concentration in T80 is increased (Figure 8). As the averaged contact angle is getting close to 90° at the larger surfactant concentration, provided the stochastic nature if this parameter, it can exceed this value for a significant amount of μ-particles, which are no longer sustained at the interface, hence decreasing their number.

The surface tension evolution during campaign 1 (C_{T80} = 0.011 g/L, Figure 18a) suggests that the particles inside the drop transport additional contaminants to the film interphases, but the nature of this surfactant is unclear. This surfactant may be T80 since particles transport it adsorbed on its surface, but this interpretation is problematic. Figure 18a shows that the WO interphase is oversaturated of Tween 80, because the surface tension is well below the equilibrium value most of the time (σ_{eq} = 13.1 mN/m for the T80 concentration of the experiment). The T80−water solution with μ-particles of the drops was prepared prior to the filling of the coalescence chamber (the beginning of the experiment). This implies that T80 adsorbed in the particle surface is in equilibrium with the T80−water solution at the selected T80 concentration. Therefore, we would expect T80 to migrate from the oversaturated WO interface to the water drop or to the particle surface (in equilibrium) increasing the surface tension of the water−oil interphase contrary to observations (Figure 18). In this case, the only possibility is an equilibrium surface excess of the GO interphase smaller than the corresponding value of the GW boundary. Thus, when particles at equilibrium attach to the film surface (Figure 21b), the GO interphase releases the surplus of surfactant, which can adsorb on the film WO interphases. However, data in Figure 22 suggest a strong adsorption of T80 on the GO interphase.

The other scenario is other unknown surfactant adhered to the particle surface. This contaminant should dissolve only on the oil phase because the T80−water solution did not remove it from the particle surface. No chemical analysis was performed to detect the presence of this hypothetical new contaminant.

4.2. Film Drainage. Several simplified models[18,19,40] as well as theory[15] and simulations[41] have been proposed in the literature to predict the film-thinning rate, based on lubrication approximation.

For the proper use of viscous flow theory, both film interfaces should be immobile in the tangential direction. That is, they must absorb the tangential stresses caused by viscosity. Marangoni forces due to gradients of surface excess are the only mechanism that can resist the viscous actions. However, following Lee and Hodgson[15] and Traykov and Ivanov,[42] when the surfactant is soluble in the coalescing phase, the gradients of interfacial tension are greatly reduced due to the diffusion of surfactants from the inner part of the drop and the water bulk to both film interfaces. In that case, bulk tangential stresses are equal at both sides of the interface, which becomes mobile when Marangoni effects are canceled out. Therefore, the film drainage rate should be close to that observed between pure liquids.

In the opposite case, when the surfactant only dissolves in the film phase, the film cannot supply enough amounts of contaminants to both interfaces. Therefore, Marangoni effects quickly develop, opposing the film drainage. This situation, which is close to the case of immobilized interface, leads to drainage rates several orders of magnitude smaller than the film-thinning rate between pure liquids.

In the present study, the main surfactant (Tween 80) is preferentially soluble in the water (drop) phase, suggesting that the interface could behave as a fully mobile interface.

To summarize, there are two asymptotic limits: fully mobile and immobile interfaces. In the Supporting Information, the film drainage is solved for the case of immobile interfaces and weakly submerged drops. Using this solution, we provide a new estimator of the characteristic time for the film draining (eqs S7 and S8 in the Supporting Information) that is more accurate than previous models. In addition, we also present a simplified model for the case of fully mobile film boundaries and the estimation of the drainage time in that case (eq S18 in the Supporting Information). For immobile interfaces, we evaluate the drainage time as the time taken for the film to thin down to 10 nm. This value roughly corresponds to the action range of attractive van der Waals forces, as a possible mechanism leading to film rupture. We obtained a drainage time of about 10^{10} s for an immobile film condition and less than 1 s for a fully mobile interface, both being out of the experimental range (several tens of seconds). We can then conclude that the single action of van der Waals attraction does not cause the film breakage.

The observed two-step process of the film drainage seems to correspond to each of the aforementioned drainage regimes. First, the initial thick film is observed to remain quasi-static during the first some seconds. The development of a concentration gradient at the film rim due to interface deformation and the drop settling after the injection will generate a Marangoni stress immobilizing both film boundaries. This stage would correspond to the case of immobile interfaces with a slow drainage rate. In the same time, the molecular diffusion from the water bulk and from the droplet will compensate the default of surfactant in the central part of the film, tending to cancel *locally* the concentration gradient, and consequently the Marangoni stress. Such a process is likely to develop zones of fast and slow drainage rates, leading to the occurrence of asymmetric drainage and of Marangoni flow instabilities as observed in the second stage of the drainage process.

However, the trend displayed in Figure 6 calls for an explanation. Indeed, film drainage models predict the opposite trend, an increase of the drainage time with the drop diameter.

A tentative explanation could be related to the competition between the development of concentration gradient on the interface and the surfactant diffusion from the bulk. Increasing the drop diameter increases the film surface area where the diffusion is effective, whereas the maximum concentration gradient is always confined at the film periphery. This would lead to an earlier occurrence of the fast drainage rate stage, explaining the decreasing trend of the drainage time with increasing drop diameter.

4.3. Film Rupture Mechanism. Experimental data suggest that Tween 80 adsorbs onto the glass particles, inhibiting the bridging mechanism. The related mechanism of the film rupture should account for the randomness of the coalescence times, the "no-aging" of the oil film, at least for the largest tested concentration of T80, and the dependence of the latency period with the concentration of the added Tween 80. The film drainage until a critical film thickness does not explain this random behavior because it is a deterministic process.

Following the ideas of Kashchiev and Exerowa,[27] random molecular fluctuations seem to be the only mechanism responsible for film rupture. Due to these random fluctuations, the surface excess of Tween 80 may decrease substantially in a small area of the film surface during a short time interval, forming a "hole" of surfactant. If this hole is large enough, the monolayer of surfactant cannot inhibit the attractive van der Waals forces, giving birth to a pinhole in the oil film (Figure 23). However, for small holes, the Marangoni forces will
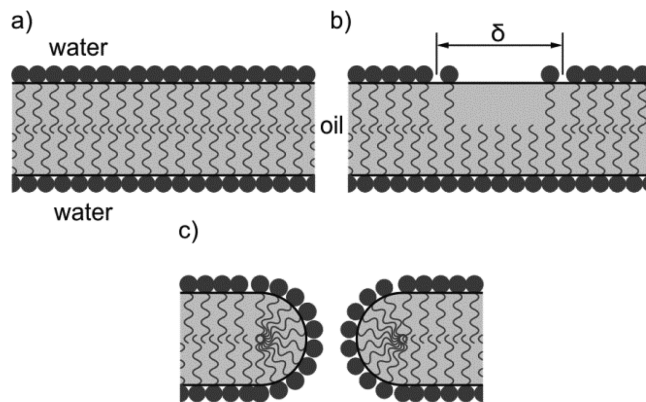
Figure 23. Film rupture mechanism: (a) uniform state of film covered by monolayers; (b) hole formation; (c) onset of film rupture.

quickly fill the hole with surfactant again and the system then recovers its initial state. This explains the memoryless property of coalescence event. Time intervals between births of holes of critical size follow a Poisson process, and the coalescence time distribution exhibits an exponential shape. De Gennes[28] argues that the critical size of those holes should be comparable to the characteristic length scale of the area occupied by a surfactant molecule adsorbed on the interface.

The calculation of the energy barrier ΔG_{max} and the size of the critical hole δ is quite difficult. An accurate knowledge of the molecular interactions and structuration of the monolayer is required. De Gennes[28] gave an estimation of ΔG_{max} as the work required to remove the surfactant over the hole surface:

$$\Delta G_{max} \sim \delta^2 \Pi \qquad (4)$$

where Π is the surface pressure $\sigma_0 - \sigma(c_{T80})$, with $\sigma_0 = \sigma(c_{T80}=0)$. Arguments derived from statistical mechanics give

the average time to generate a critical hole, which is equal to the mean coalescence time.

$$\tau_c = \tau_0 \exp\left(\frac{\Delta G_{max}}{k_B T}\right) \tag{5}$$

k_B is the Boltzmann constant and T is the temperature. The pre-exponential factor τ_0 is a characteristic time scale of hole formation, which depends on the film area that can nucleate holes.

$$\tau_0 \sim \frac{1}{f_n S_{eff}} \tag{6}$$

S_{eff} is the area of the film prone to break, and f_n is the hole nucleation frequency per unit surface. The unitary hole nucleation frequency depends on the chemical composition of the interphase, scaling with characteristic times of the molecular interactions (e.g., the number of molecular collisions per unit time, frequencies of some molecular vibration modes, etc.). Thus, the calculation of f_n requires the use of computing expensive molecular dynamics. Deminiere et al.[43] propose a way to estimate it using macroscopic properties of the involved media. However, this approach is not directly connected to the real physics driven nucleation processes.

Mean coalescence time is roughly independent of the drop diameter (Figure 10), suggesting that S_{eff} depends weakly on the drop. Assuming also that f_n varies slowly with the surface excess, the ratio of the mean coalescence time of both campaigns (τ_{C1} and τ_{C2}) provides an estimation for the size of the critical hole.

$$\frac{\tau_{C1}}{\tau_{C2}} \sim \exp\left(\delta^2 \frac{\Pi_1 - \Pi_2}{k_B T}\right) = \exp\left(\delta^2 \frac{\sigma_2 - \sigma_1}{k_B T}\right) \tag{7}$$

Using the equilibrium values of surface tension for both T80 concentration, eq 7 provides an estimated size for the critical holes, $\delta \sim 10$ Å. This order of magnitude must be compared with a characteristic length scale of the adsorbed molecule of Tween 80.

Figure 24 shows a graphical representation of the molecular structure of Tween 80. The Tween 80 molecule has four
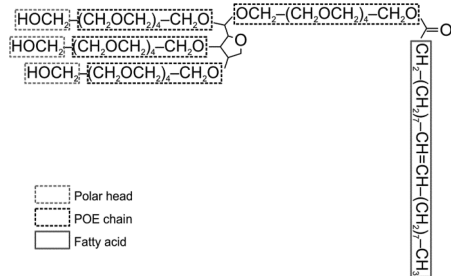

Figure 24. Molecular structure of polysorbate 80.

polyoxyethylene (POE) hydrophilic chains and a hydrophobic oleic acid attached to the end of one POE chain. Amani et al.[44] used a molecular dynamics based method to simulate the average lengths of the POE chains and at the tail to give 14.63 ± 0.99 and 12.40 ± 2.09 Å, respectively. The corresponding size of the fatty acid is 18.7 ± 5.35 Å. The size of the critical hole estimated from eq 5 well compares with the size of the oleic acid chain, validating the hypothesis of de Gennes' model.[28]

Note that the hole nucleation theory leading to eq 5 predicts a huge variation of the coalescence time for a tiny variation of the critical hole size δ because of the exponential function and cannot be considered as a predictive model for the mean coalescence time. In addition, the size of the critical hole should depend on the surface excess of the interphase. Even though it is not predictive, it provides a physically grounded tool to understand the hole nucleation process in energy barrier limited coalescence.

This model, however, in its construction, applies for the general case of the rupture of film fluid interfaces, uniformly covered by a surfactant monolayer. An interesting question is the effect of the particles on the interfaces upon the parameters of this model. If the energy barrier is assumed to remain unaffected, the time scale for a critical hole to grow on a particle surface is probably orders of magnitude larger than on a fluid interface. Therefore, it could be inferred that, in this case, significant adsorption of surfactant on the particle surface not only inhibits the bridging mechanism but also delays the occurrence of critical size hole formation and its subsequent growth. However, as the amount of particles considered in these studies is always small, the mean coalescence time is not sensitive to this retardation effect. With a significant covering of the interface by the particles, the dominant effect would then probably be the particle-induced repulsive effect observed in Pickering emulsions.

4.4. Film Retraction and Bending. Since the retraction is driven by the surface tension, it is closely connected to the adsorption of surfactants at the film interfaces. The analysis of the film retraction stage is therefore motivated by the fact that it provides relevant information about the state of the film interfaces at the film rupture.

Figure 17 shows that the asymptotic retraction velocity of the film varies between 0.2 and 0.8 m/s for the lower surfactant concentration whereas it remains nearly constant (about 0.5 m/s) for the higher one. The film reaches its limit velocity in less than 1 ms. When film retraction is dominated by inertia and interfacial tension,[45] the final retraction velocity of an axisymmetric film is known as the Taylor−Culick speed v_{TC}:

$$v_{TC} = \sqrt{\frac{2\sigma}{\rho h}} \tag{8}$$

In the foregoing expression, h and ρ are the thickness and the bulk density of the film, respectively. However, this expression is not consistent with the measured values of retraction velocity of the order of 1 m/s. According to eq 8, this value would correspond to a 100 μm thick film, a much too high value for the film rupture to occur.

A second hypothesis is that the film retraction is controlled by viscous forces instead of inertia. In this scenario, the retraction velocity should scale with the ratio of the interfacial tension to the viscosity ($v \sim \sigma/\mu$). This corresponds to velocities of about 40 and 20 mm/s for the first and second campaigns, respectively. These velocities are 1 order of magnitude smaller than the actual results. Therefore, neither inertia nor viscous forces can explain the observed retraction speed.

De Malmazet et al.[29] observed that the film around the hole bends during its retraction and that bending was ascribed to the difference of interfacial tension between the upper and the lower sides of the film. We also observe this bending in campaign 1. Figure 25 shows a significant bending for drops

Figure 25. Bending of the hole limit for different coalescence times. Campaign 1, C_{T80} = 0.011 g/L.

with short coalescence time (t_C = 169 s), which is strongly attenuated for older drops (t_C = 1562 s). The drag acting on the bent rim would then control the retraction speed: the larger the bending, the larger the drag and the slower the velocity of retraction. For the larger surfactant concentration (campaign 2), the film bending seems to be less pronounced for the younger drops (Figure 26, left) and also tends to
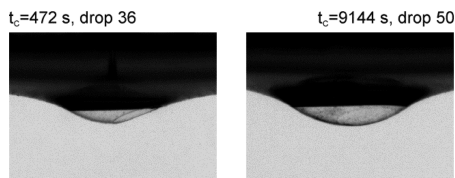

Figure 26. Bending of the hole limit for different coalescence times. Campaign 2, C_{T80} = 0.11 g/L.

diminish with older drops (Figure 26, right). Therefore, in that case, the effect of this bending on the retraction speed becomes weakly correlated to the drop age resting on the interface (before coalescence).

The most plausible mechanism for the film bending occurrence during retraction is the difference of interfacial tension between both interfaces of the film. As the film was observed to bend downward the lower side of the film, the interfacial tension of the lower side should then be larger than that of the upper side, implying a larger amount of surfactants in the upper interface. As initial concentrations of Tween 80 in the drop and in the water bulk are the same, the new input of surfactants can only be transported by the particles that are likely to release them on the upper film interface during the latency period. This additional supply in surfactants by the particles explains the direction of bending observed. In de Malmazet's experiments, such an input in surfactants on the upper interface by the particles was absent and the surface tension of the injected drops (with a new interphase clean of surfactants) was always larger than that of the plane oil−water interface (with an older interphase covered by contaminants after an adsorption process), resulting in a film bending oriented upward, in the opposite direction as that observed in this study. These two experiments tend to confirm that, on one hand, the bending phenomenon is likely to be driven by the surface tension differences between the film interfaces and, on the other hand, glass μ-particles adsorb surfactants.

In both campaigns, the film bending diminishes with the coalescence time, indicating that the difference of interfacial tension and surface excess between both sides of the film decreases with the drop age. The surfactant input from the microparticles and slowly released on the film upper side is able to diffuse to the lower side during the latency period where the film thickness is probably of the order of the size of a few surfactant molecules. This migration is also responsible for

the decrease of interfacial tension between the beginning and the end of each day (Figure 18b). During the night, the surface-active contaminants desorb diffusing into the liquid volume and increasing the surface tension.

During the second campaign (with a bulk concentration 10 times larger than in the first campaign), the interface is closer to saturation, reducing greatly the surface tension and masking the effect of the surfactants supplied by the μ-particles. As a consequence, the daily adsorption−desorption cycle that was observed during campaign 1 seems to vanish (Figure 18). Also, there is a significant reduction in the difference of interfacial tension between the surfaces of the film, resulting in a visible attenuation of the bending. This explains why the retraction velocity becomes independent of the coalescence time in this case (Figure 17).

The difference between the two campaigns is therefore not limited to the difference in bulk surfactant concentration but is also characterized by the difference of the surface concentration across the film thickness that develops during the latency period. This surface excess difference is generated by the supply in surfactants adsorbed on the glass particles contained in the injected drops. It is more pronounced with the lower surfactant concentration because an input of surfactants has a stronger effect well below than close to the interface saturation. It also provides an explanation of the differences observed between the coalescence time cumulative distribution functions (CDFs) of campaigns 1 and 2. In campaign 2, the energy barrier and the surface tension vary little with time, so the coalescence events are well-characterized by a Poisson process with a constant coalescence rate. In campaign 1, the generation of an initial significant vertical surfactant concentration profile makes the surface tension decrease and the energy barrier increase as the coalescence time, and therefore the age of the interface, is increasing. This time evolution of the film interfaces is responsible for the decreasing coalesce rate described by the piecewise exponential (cf. eq 2 and Table 2).

The surface excess difference between upper and lower film interfaces is negative, causing a downward oriented bending of the film during the film rupture. In de Malmazet's experiments, this difference was positive and the bending was oriented upward. This difference of film bending orientation could explain the depletion of particles in the impact zone that was observed in the present experiments, and not in de Malmazet's experiments. An upward bending is probably associated with a tangential velocity oriented upward as well, that will transport surfactants and particles from the hole rim toward the top (apex) of the coalescing drop, leaving an impact zone loaded with particles at the end of the coalescence. On the contrary, a downward bending will transport the μ-particles from the hole rim toward the oil−water plane interface, leading to an impact zone depleted in particles.

5. CONCLUSION

Coalescence of millimeter-sized water drops with an oil−water interface has been investigated in the presence of both water-soluble nonionic surfactant (Tween 80) and hollow glass μ-particles at the interfaces. Two substantial concentrations of surfactant have been considered, respectively corresponding to interfaces loaded with monolayers well below and close to saturation.

Coalescence involves two consecutive mechanisms: the drainage of the continuous phase film between both drops,

ruled by macroscopic fluid mechanics, and the final film rupture at nanometric scales, which is controlled by molecular interactions. Thus, the coalescence time is the sum of the duration of both processes.

When both film interphases are unstable (i.e., the two facing surfaces are attractive), the film rupture is much faster than its previous drainage. In this case, the coalescence process becomes deterministic and controlled by the film drainage.

Otherwise, when the interphases are metastable (i.e., molecular forces are repulsive), the time scale of the rupture is much larger than the characteristic time of the drainage. This is the case of a film stabilized by a bilayer of surfactants. De Gennes[28] proposed that molecular fluctuations should generate a hole in the surfactant monolayer and cause the film rupture. This event, which can last a very long time depending on the magnitude of the involved energy barrier, follows a stochastic Poisson process whose time constant is a function of the molecular properties of the film surfaces.

In most industrial applications, the fluid system is complex and involves both surfactants and fine solid particles that adsorb on the interfaces. In the previous work of de Malmazet et al.,[29] authors studied the coalescence between interfaces loaded with microparticles, which are preferentially wetted by the water (drop) phase. It was shown that microparticles lying on the film interfaces did promote the film rupture and subsequent coalescence through a bridging mechanism. Observed coalescence times were deterministic as they are controlled by the time for the film to drain until a thickness that compares with particle size.

In the present work, it is shown that the addition of a significant concentration of a nonionic surfactant (Tween 80) stabilizes the interstitial film. The surfactant adsorbs on the particles, inducing repulsive interactions between the particle surfaces and the film interfaces as in the case of a liquid film simply loaded with surfactants (steric repulsion of hydrophobic chains). It turned out that coalescence becomes a Poisson process, limited by the energy barrier of the surfactant monolayer. The coalescence time increases with the surfactant concentration because the energy barrier also increases, and the hole nucleation rate decreases.

Another interesting result is the modulation of the film drainage process. It was shown that it is a stepwise process, starting with a slow drainage rate stage where the development of Marangoni stresses during interface deformation will tend to immobilize the film interfaces. When diffusive transport of surfactants from the liquid bulk to the interfaces has locally canceled the concentration gradients, the film drainage rate is strongly accelerated and driven by Marangoni flow instabilities. The competition between these two counteracting effects could be responsible for the observed decay of the drainage time with the drop diameter, which is the trend opposite to that predicted by classical theories.

In addition, the Marangoni effect is also involved in the film retraction after film rupture. The differences of surface tension on both sides of the film interfaces is responsible for film bending at the hole rim, which in turn controls its retraction speed during drop coalescence. With the larger concentration of T80, this surface tension difference is reduced, and the film bending is strongly attenuated.

The surfactants adsorbed on the μ-particles have other consequences on the coalescence mechanisms. Being transported by the drops loaded with surfactants, they provide a supplementary input of contaminants at the film upper interface, developing a vertical gradient of surface excess across the film thickness. This gradient, which slowly diffuses with time on both film interfaces, tends to decrease the coalescence rate with time for T80 concentration well below saturation (campaign 1). It is also responsible for the downward orientation of film bending during film rupture, which in turn is believed to cause the depletion of μ-particles observed in the impact zone after coalescence has ended.

To summarize, experiments carried out in this study bring to light the intricate mechanisms involved in the coalescence process of complex interfaces, loaded with contaminants, surfactants, and μ-particles. Without surfactants, de Malmazet's experiments have unveiled the μ-particle-induced bridging effect, leading to a faster and drainage-controlled coalescence rate. In the present work, it was shown that loading a water–oil interface with a monolayer of surfactants (at a significant concentration) and μ-particles inhibits the bridging effect when the surfactant can adsorb on the μ-particles. In this case, coalescence is no longer driven by the drainage stage, but is an energy barrier limited stochastic process, the time constant of which is a growing function of the surface excess of the monolayer.

■ ASSOCIATED CONTENT

ⓈSupporting Information

The Supporting Information is available free of charge on the ACS Publications website at DOI: 10.1021/acs.iecr.9b02524.

Mathematical models of the film drainage: analytical solution for the immobile interphases case and order-of-magnitude analysis for mobile boundaries (PDF)

■ AUTHOR INFORMATION

Corresponding Author
*E-mail: esteban.calvo@unizar.es.

ORCID ⊙
Esteban Calvo: 0000-0002-5631-1401
Frédéric Risso: 0000-0002-8380-4957

Present Address
#Erik de Malmazet: Électricité de France R&D, Département Mécanique des Fluides, Energie et Environnement (MFEE), 78401 Chatou Cedex, France.

Author Contributions
The manuscript was written through contributions of all authors. All authors have given approval to the final version of the manuscript. All authors contributed equally.

Notes
The authors declare no competing financial interest.

■ REFERENCES

(1) Santolaya, J. L.; García, J. A.; Calvo, E.; Cerecedo, L. M. Effects of Droplet Collision Phenomena on the Development of Pressure Swirl Sprays. *Int. J. Multiphase Flow* **2013**, *56*, 160−171.
(2) Mahajan, L. D. Flüssige Tropfen an der Oberfläche Derselben Flüssigkeit. *Eur. Phys. J. A* **1933**, *84*, 676.
(3) Mahajan, L. D. Über die Lebensdauer von Flüssigen Tropfen auf der Oberfläche der Gleichen Flüssigkeit. *Colloid Polym. Sci.* **1934**, *69*, 16.

(4) Cockbain, E. G.; McRoberts, T. S. The Stability of Elementary Emulsion Drops and Emulsions. *J. Colloid Sci.* **1953**, *8*, 440−451.

(5) Gillespie, T.; Rideal, E. K. The Coalescence of Drops at an Oil-Water Interface. *Trans. Faraday Soc.* **1956**, *52*, 173−183.

(6) Elton, G. A. H.; Picknett, R. G. The Coalescence of Aqueous Droplets with an Oil/Water Interface. *Second International Congress of Surface Activity*; Butterworths: London, 1957: Vol. 1, pp 288−294.

(7) Charles, G. E.; Mason, S. G. The Mechanism of Partial Coalescence of Liquid Drops at Liquid/Liquid Interfaces. *J. Colloid Sci.* **1960**, *15*, 105−122.

(8) Charles, G. E.; Mason, S. G. The Coalescence of Liquid Drops with Flat Liquid/Liquid Interfaces. *J. Colloid Sci.* **1960**, *15*, 236−267.

(9) Mohamed-Kassim, Z.; Longmire, E. K. Drop Coalescence through a Liquid/Liquid Interface. *Phys. Fluids* **2004**, *16*, 2170−2181.

(10) Scheludko, A. Über die Zerreißwahrscheinlichkeit von Schaumfilmen aus Isoamylalkohollösungen. *Z. Elektrochem.* **1957**, *61*, 220−222.

(11) Hartland, M. A. The Coalescence of a Liquid Drop at a Liquid-Liquid Interface. Part I: Drop Shape. *Trans. Inst. Chem. Eng.* **1967**, *45*, 97−101.

(12) Hartland, M. A. The Coalescence of a Liquid Drop at a Liquid-Liquid Interface. Part II: Film Thickness. *Trans. Inst. Chem. Eng.* **1967**, *45*, 102−108.

(13) Hartland, M. A. The Coalescence of a Liquid Drop at a Liquid-Liquid Interface. Part III: Film Rupture. *Trans. Inst. Chem. Eng.* **1967**, *45*, 109−114.

(14) Hartland, M. A. The Coalescence of a Liquid Drop at a Liquid-Liquid Interface. Part IV: The Effect of Surface Active Agent. *Trans. Inst. Chem. Eng.* **1967**, *45*, 275−282.

(15) Lee, J. C.; Hodgson, T. D. Film Flow and Coalescence-I. Basic Relations, Film Shape and Criteria for Interface Mobility. *Chem. Eng. Sci.* **1968**, *23*, 1375−1397.

(16) Hodgson, T. D.; Lee, J. C. The Effect of Surfactants on the Coalescence of Drop at an Interface. I. *J. Colloid Interface Sci.* **1969**, *30*, 94−108.

(17) Hodgson, T. D.; Woods, D. R. The Effect of Surfactants on the Coalescence of Drop at an Interface. II. *J. Colloid Interface Sci.* **1969**, *30*, 429−446.

(18) Lang, S. B.; Wilke, C. R. A Hydrodynamic Mechanism for the Coalescence of Liquid Drops. I. Theory of Coalescence at a Planar Interface. *Ind. Eng. Chem. Fundam.* **1971**, *10*, 329−340.

(19) Lang, S. B.; Wilke, C. R. A Hydrodynamic Mechanism for the Coalescence of Liquid Drops. II. Experimental Studies. *Ind. Eng. Chem. Fundam.* **1971**, *10*, 341−352.

(20) Basheva, S.; Gurkov, T. D.; Ivanov, I. B.; Bantchev, G. B.; Campbell, B.; Borwankar, R. P. Size Dependence of the Stability of Emulsion Drops Pressed against a Large Interface. *Langmuir* **1999**, *15*, 6764−6769.

(21) Chen, X.; Mandre, S.; Feng, J. J. 2006. Partial Coalescence between a Drop and a Liquid-Liquid Interface. *Phys. Fluids* **2006**, *18*, 051705.

(22) de Vries, A. J. Foam Stability. Part I. Structure and Stability of Foams. *Recl. Trav. Chim. Pays-Bas* **1958**, *77*, 81−91.

(23) de Vries, A. J. Foam stability. Part. II. Gas diffusion in foams. *Recl. Trav. Chim. Pays-Bas* **1958**, *77*, 209−223.

(24) de Vries, A. J. Foam stability. Part. III. Spontaneous Foam Destabilization Resulting from Gas Diffusion. *Recl. Trav. Chim. Pays-Bas* **1958**, *77*, 283−296.

(25) de Vries, A. J. Foam stability. Part IV. Kinetics and Activation Energy of Film Rupture. *Recl. Trav. Chim. Pays-Bas* **1958**, *77*, 383−399.

(26) de Vries, A. J. Foam stability. Part V. Mechanism of Film Rupture. *Recl. Trav. Chim. Pays-Bas* **1958**, *77*, 441−461.

(27) Kashchiev, D.; Exerowa, D. Nucleation Mechanism of Rupture of Newtonian Black Films. I. Theory. *J. Colloid Interface Sci.* **1980**, *77*, 501−511.

(28) De Gennes, P. G. Some Remarks on Coalescence in Emulsions or Foams. *Chem. Eng. Sci.* **2001**, *56*, 5449−5450.

(29) de Malmazet, E.; Risso, F.; Masbernat, O.; Pauchard, V. Coalescence of Contaminated Water Drops at an Oil/Water Interface: Influence of Micro-Particles. *Colloids Surf., A* **2015**, *482*, 514−528.

(30) Braun, A. C.; Ilko, D.; Merget, B.; Gieseler, H.; Germershaus, O.; Holzgrabe, U.; Meinel, L. Predicting Critical Micelle Concentration and Micelle Molecular Weight of Polysorbate 80 Using Compendial Methods. *Eur. J. Pharm. Biopharm.* **2015**, *94*, 559−568.

(31) Grillo, I.; Penfold, J.; Tucker, I.; Cousin, F. Spontaneous Formation of Nanovesicles in Mixtures of Nonionic and Dialkyl Chain Cationic Surfactants Studied by Surface Tension and SANS. *Langmuir* **2009**, *25*, 3932−3943.

(32) Penfold, J.; Thomas, R. K.; Li, P. X.; Petkov, J. T.; Tucker, I.; Webster, J. R. P.; Terry, A. E. Adsorption at Air−Water and Oil−Water Interfaces and Self-Assembly in Aqueous Solution of Ethoxylated Polysorbate Nonionic Surfactants. *Langmuir* **2015**, *31*, 3003−3011.

(33) Miyamura, A.; Iwasaki, S.; Ishii, T. Experimental Wall Correction Factors of Single Solids Spheres in Triangular and Square Cylinders, and Parallel Plates. *Int. J. Multiphase Flow* **1981**, *7*, 41−43.

(34) Princen, H. M. Shape of a Fluid Drop at a Liquid-Liquid Interface. *J. Colloid Sci.* **1963**, *18*, 178−195.

(35) Jones, A. F.; Wilson, S. D. R. The Film Drainage Problem in Droplet Coalescence. *J. Fluid Mech.* **1978**, *87*, 263−288.

(36) Bogdanova, Y. G.; Dolzhikova, V. D.; Summ, B. D. Wetting of Solids by Aqueous Solutions of Surfactant Binary Mixtures: 2. Wetting of High-Energy Surface. *Colloid J.* **2003**, *65*, 290−294.

(37) Cucakovich, N. B. Determination of Tween 80 in Tissue Culture Media, Vaccines, and Related Products. *Anal. Biochem.* **1971**, *40*, 183−186.

(38) Furlong, D. N.; Aston, J. R. Adsorption of Polyoxyethylated Nonyl Phenols at Silica/Aqueous Solution Interfaces. *Colloids Surf.* **1982**, *4*, 121−129.

(39) Nevskaia, D. M.; Guerrero-Ruiz, A.; López-González, J. de D. Adsorption of Polyoxyethylenic Surfactants on Quartz, Kaolin, and Dolomite: A Correlation between Surfactant Structure and Solid Surface Nature. *J. Colloid Interface Sci.* **1996**, *181*, 571−580.

(40) Chevaillier, J. P.; Klaseboer, E.; Masbernat, O.; Gourdon, C. Effect of Mass Transfer on the Film Drainage between Colliding Drops. *J. Colloid Interface Sci.* **2006**, *299*, 472−485.

(41) Klaseboer, E.; Chevaillier, J. P.; Gourdon, C.; Masbernat, O. Film Drainage between Colliding Drops at Constant Approach Velocity: Experiments and Modeling. *J. Colloid Interface Sci.* **2000**, *229*, 274−285.

(42) Traykov, T. T.; Ivanov, I. B. Hydrodynamics of Thin Liquid Films. Effect of Surfactants on the Velocity of Thinning of Emulsion Films. *Int. J. Multiphase Flow* **1977**, *3*, 471−483.

(43) Deminiere, B.; Colin, A.; Leal-Calderon, F.; Muzy, J. F.; Bibette, J. Cell Growth in a 3D Cellular System Undergoing Coalescence. *Phys. Rev. Lett.* **1999**, *82*, 229−232.

(44) Amani, A.; York, P.; de Waard, H.; Anwar, J. Molecular Dynamics Simulation of a Polysorbate 80 Micelle in Water. *Soft Matter* **2011**, *7*, 2900−2908.

(45) Savva, N.; Bush, L. W. M. Viscous Sheet Retraction. *J. Fluid Mech.* **2009**, *626*, 211−240.